Microscopic-balance-equation theory of the real-space transfer in semiconductor multiple quantum wells

P. Kleinert and M. Asche
Paul-Drude-Institut für Festkörperelektronik, Hausvogteiplatz 5-7, 10117 Berlin, Federal Republic of Germany
(Received 15 April 1994)

Hot-electron effects in a multiple-layer system are treated as a function of a parallel electric field on the basis of a microscopic-balance-equation theory. Dynamically screened intrasubband scattering on ionized impurities, acoustical phonons due to deformation potential and piezoelectric interaction, as well as polar optical phonons are taken into account. The real-space transfer of electrons into the region between the layers is described by transfer scattering on optical and acoustical phonons. The obtained field-dependent drift velocities, electron temperatures, and densities of the two electronic subsystems are analyzed by considering the energy loss rates and frictional-force contributions of the included scattering events. Analytical expressions are derived for the transfer-scattering contributions to the energy and force balance and the phonon assisted electron-density transfer. Specific results are obtained for a multiple-quantum-well system, which we compare with our former, more phenomenological, approach applied to analyze experimental results of multiple δ layers in GaAs.

I. INTRODUCTION

Nonlinear transport in semiconductor materials has received much interest from both the experimental and theoretical points of view. In the last decade, interest has turned to investigation of hot electrons in semiconductor heterostructures. For systems consisting of several carrier subsystems the treatment of nonlinear transport is complicated by cross-correlation terms due to the carrier transfer mechanisms. It is known[1–5] that an electronic real-space transfer can cause a negative differential conductivity if the mobility in the barriers is lower than in the wells. However, depending on the changes of charge density and potential distribution involved, the transfer process can diminish the negative differential conductivity caused by electron transfer between band edges with different effective masses (e.g., in GaAs $\Gamma \rightarrow L, X$).

Most theoretical investigations of nonlinear transport phenomena rely on Monte Carlo simulations or the solution of the semiclassical Boltzmann equation. An alternative analytical Green's function theory has been developed by Lei and Ting[6] in order to study the nonlinear transport in various semiconducting materials. In this approach, balance equations were derived by separating the center of mass from the relative motion of electrons and treating the density matrix of the system to first order in the electron scattering on impurities and phonons. The balance equations for momentum and energy were solved by using a parametrized distribution function of Fermi type, which is appropriate if there is a rapid carrier-carrier interaction for the thermalization to an electron temperature and the formation of an effective drift velocity. The approach had been applied to various interesting hot-electron transport phenomena and has already demonstrated its reliability and practicability.[7,8]

The purpose of the present paper is to extend the microscopic Green's function theory to treat electron transitions between confined and extended states as implemented in the real-space transfer in multiple quantum wells (MQW's) and superlattice systems. The electrons in the confined and extended states are treated as separate subsystems—an assumption justified for weak electron-electron scattering between them in comparison to the collisions within each subsystem. This assumption is in accordance with the general observation that intrasubband transitions are usually more pronounced than intersubband processes. This is due to the more severe restrictions with respect to the possible final states because of momentum and energy conservation for intersubband as well as intervalley transitions in comparison to intraband scattering processes. A quantitative treatment of the intersubband Coulomb scattering would put our approach on a firmer basis, but this is beyond the scope of the present paper, since the degenerate density of the two-dimensional electrons terms proportional to the product of four distribution functions appears in the balance equations.

In an electric field parallel to the layers, the electrons, which are primarily confined in the potential wells, may acquire enough energy to be transferred to the region between the layers. We consider the special case that the impurity concentration in the interlayer space is much lower than the equivalent concentration within the wells and the subsequent increase in mobility is not compensated by an increase of the effective masses.

We had treated this real-space transfer both experimentally and theoretically already in Refs. 9 and 10 for the special system of multiple δ layers in GaAs. We focused our attention on the effects of scattering events and did not consider the details of the potential profile. This approximation is also adopted here. In comparison to our former approximate treatment, we now

develop a full microscopic theory of the real-space transfer process by including microscopic mechanisms for the exchange of particles between the two different groups of electrons. This adequate treatment of the electron transfer processes also allows us to remove the restriction to low electric fields, which was necessary in our former approach.[9,10] Methodologically, the particle balance approach for the real-space transfer resembles the treatment of intervalley transfer in $\mathbf{k}$ space.[11,12]

By separating the center of mass from the relative motion of essentially two- and three-dimensional types of carriers (2D and 3D), treating the center-of-mass motion classically and introducing two electron temperatures and quasichemical potentials for the two subsystems, we derive a set of balance equations for the force, energy, and particle exchange to determine 2D and 3D drift velocities and populations of the two subsystems in the steady state.

II. THE HAMILTONIAN

Let us consider an essentially two-dimensional subsystem of electrons within a periodic square well potential (type 1) together with its more or less three-dimensional counterparts (type 2) above the barrier, as schematically shown in Fig. 1. The electric field E is aligned parallel to the wells and perpendicular to the z axis, which is chosen in the direction of the periodic potential. In this paper, we consider the special case that the sheet separation d is much greater than the well width a so that electron tunneling through the barriers and the energetic width of the quantum well subbands can be neglected. That means that electrons in different wells decouple, as is characteristic for a multiple quantum well system. Furthermore, we assume that within the wells there is only one relevant energy level separated by E_c from the top of the barrier. Of course, our treatment can be extended to more confined levels in principle; however, the numerical effort to solve the system of coupled equations increases considerably in this case.

A suitable starting point for the theoretical description is the second quantized Hamiltonian in the coordinate representation, where the center-of-mass degrees of freedom have already been separated from the relative coordinates. The total Hamiltonian

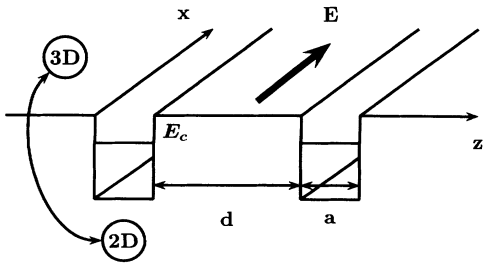

FIG. 1. Schematic diagram of the considered two-carrier subsystems.

$$H = H_T + H_F + H_{1e} + H_{2e} + H_{\rm ph} + H_I \tag{2.1}$$

of the two subsystems 1 and 2 which are in a stationary nonequilibrium state include the kinetic (H_T) and potential (H_F) energy of the center-of-mass motion in a constant electric field as well as the electronic contributions (H_{1e} and H_{2e}), which depend on the relative coordinates, and the interaction term (H_I) connected with the electron scattering on impurities, phonons, and other electrons. For simplicity we assume that the bulk phonon spectrum ($H_{\rm ph}$) is not changed by the superlattice potential, i.e., we restrict the model to quantum well widths, for which the interface contribution can be neglected.[13,14] In the single electron picture the electronic states in the rectangular potential wells can be characterized by the wave function

$$\varphi_{l\,\mathbf{k}_\parallel}(\mathbf{r}_\parallel, z) = e^{i\,\mathbf{k}_\parallel\cdot\mathbf{r}_\parallel}\,\zeta[z - l\,(d+a)]\,, \tag{2.2}$$

which depends on the layer index l and a two-dimensional wave vector $\mathbf{k}_\parallel = (k_x, k_y)$. The envelope function of the lowest subband can be approximated by

$$\zeta(z) = \begin{cases} (2/a)^{1/2}\,\cos(\pi z\,/a), & -a/2 \le z \le a/2 \\ 0, \quad \text{otherwise} \end{cases} \tag{2.3}$$

and the corresponding energy

$$\varepsilon_{1k_\parallel} = \frac{\hbar^2\,\mathbf{k}_\parallel^2}{2\,m_1^*} \tag{2.4}$$

is degenerate with respect to l. Here we assumed that (i) tunneling is small enough that electrons are confined to just one well, and (ii) the width of the wells is narrow and the electron density is not too high, such that electrons occupy only one subband.

The three-dimensional electronic states are characterized by plane waves with energies given by

$$\varepsilon_{2k} = \frac{\hbar^2\,\mathbf{k}^2}{2\,m_2^*} + E_c \tag{2.5}$$

in the effective-mass approximation. In this paper we consider the special case that the effective-mass discontinuities can be neglected so that we have only one effective mass $m^* = m_1^* = m_2^*$ for 2D and 3D electrons.

Electron-impurity and electron-phonon interaction processes within each electronic subsystem (1 and 2) as well as phonon-mediated electronic transitions between them are taken into account in the interaction part

$$H_I = H_{e-i}^1 + H_{e-i}^2 + H_{e-\rm ph}^1 + H_{e-\rm ph}^2 + H_{e-\rm ph}^{12} + H_{e-\rm ph}^{21}\,. \tag{2.6}$$

More precisely, we treat scattering of electrons on ionized impurities, acoustical phonons via a deformation potential as well as piezoelectric interaction, and polar optic phonons within each electronic subensemble, but transfer processes only due to scattering on acoustical and optical phonons, whereas transfer by electron-electron collisions is neglected for simplicity. When transfer processes by

optic phonons are dominating, this approximation is justified as shown in Ref. 15, but for low electron energies it can play a role besides the transfer due to acoustic phonons.

Because of the underlying symmetries we prefer a momentum-space representation of the Hamiltonian (2.1) and (2.6) by introducing via

$$\psi_{1\sigma}(\mathbf{r}) = \sum_{\mathbf{k}_\parallel\, l} \varphi_{l\,\mathbf{k}_\parallel}(\mathbf{r}_\parallel, z)\, c_{1\mathbf{k}_\parallel\, l\sigma}, \tag{2.7}$$

$$\psi_{2\sigma}(\mathbf{r}) = \sum_{\mathbf{k}} e^{i\,\mathbf{k}\cdot\mathbf{r}} c_{2\mathbf{k}\sigma} \tag{2.8}$$

creation ($c^+_{1\mathbf{k}_\parallel l\sigma}$ and $c^+_{2\mathbf{k}\sigma}$) and annihilation ($c_{1\mathbf{k}_\parallel l\sigma}$ and $c_{2\mathbf{k}\sigma}$) operators for electrons in the relative coordinates with definite wave vectors ($\mathbf{k}_\parallel$ for type 1 and $\mathbf{k}$ for type 2) and spin σ. The resulting expressions for the type 1 and type 2 contributions of the Hamiltonian (2.1) and (2.6) had already been derived and were published in Refs. 6 and 16, respectively. The transfer between two- and three-dimensional carrier types is accounted for by microscopic scattering processes on both acoustical and optical phonons,

$$H^{12}_{e\text{-ph}} = \sum_{q\lambda} M_{12}(\mathbf{q}\lambda)\, e^{i\mathbf{q}\cdot\mathbf{R}_1}\, (b^+_{\mathbf{q}\lambda} + b_{-\mathbf{q}\lambda}) \times \sum_{\mathbf{k}_\parallel l\,\sigma} e^{i\mathbf{k}\cdot(\mathbf{R}_1-\mathbf{R}_2)}\, I_l(q_z+k_z) c^+_{1\mathbf{k}_\parallel+\mathbf{q}_\parallel l\sigma}\, c_{2\mathbf{k}\sigma}, \tag{2.9}$$

$$H^{21}_{e\text{-ph}} = \sum_{\mathbf{q}\lambda} M_{21}(\mathbf{q}\lambda)\, e^{i\mathbf{q}\cdot\mathbf{R}_2}\, (b^+_{\mathbf{q}\lambda} + b_{-\mathbf{q}\lambda}) \times \sum_{\mathbf{k}_\parallel l\,\sigma} e^{i\mathbf{k}_\parallel\cdot(\mathbf{R}_{2\parallel}-\mathbf{R}_{1\parallel})}\, I_l(-k_z) c^+_{2\mathbf{k}+\mathbf{q}\sigma}\, c_{1\mathbf{k}_\parallel l\sigma}\,. \tag{2.10}$$

Here the form factor I_l is calculated from

$$I_l(q_z) = \int dz\, \zeta(z-ld)\, e^{i\,q_z\,z}, \tag{2.11}$$

and $\mathbf{R}_1$ ($\mathbf{R}_2$) are center-of-mass coordinates of type 1 (2) electrons, respectively. $b^+_{\mathbf{q}\lambda}$ ($b_{\mathbf{q}\lambda}$) are creation (annihilation) operators for phonons of wave vector $\mathbf{q}$ in branch λ and of frequency $\omega_{\mathbf{q}\lambda}$. The matrix elements M_{12} and M_{21} of the electron-phonon interaction are assumed to agree with the corresponding ones for the intrasubband scattering. For both intrasubband and transfer scattering by deformation potential interaction of acoustic phonons the matrix element is expressed by

$$|\, M(q, ac)\,|^2 = \frac{\hbar\, E_1 q}{2\, v_s\, \rho}, \tag{2.12}$$

where E_1 is the acoustic deformation potential, ρ the mass density of the crystal, and v_s the longitudinal sound velocity. Furthermore, we include intrasubband and transfer scattering on polar optical phonons described by the Fröhlich matrix element

$$|\, M(q, op)\,|^2 = \frac{e^2}{2\,\varepsilon_0 q^2} \left(\frac{1}{\kappa_\infty} - \frac{1}{\kappa}\right) \hbar\omega_0, \tag{2.13}$$

where ω_0 is the longitudinal optical phonon frequency, κ the static dielectric constant, and κ_∞ the high-frequency dielectric constant, and $\varepsilon_0 = 1/4\pi$, respectively. In the case of heterostructure quantum wells with regard to the interaction with optical modes, the limitation to one type of bulklike phonon is appropriate for the scattering within the lowest level, for which the electron only negligibly penetrates into the barrier. This may appear as a restriction now,[13] when the transfer of electrons from the well into the states above the barrier is taken into account. However, for the considered potential created by doping profiles the assumption of one type of bulklike phonon is realized.

Piezoelectric scattering on phonons is only treated for the separated type 1 and type 2 electronic subsystems. The piezoelectric interaction is allowed for both longitudinal and transverse phonons. Since for GaAs the transverse sound velocities are lower than the longitudinal one we regard only the sum of the two independent transverse branches. This approximation is further motivated, because a longitudinal mode is already included in the contribution from the deformation potential interaction.

$$|\, M(q, \text{piez})\,|^2 = \frac{32\pi^2\hbar\, e^2 e_{14}^2}{\kappa^2\rho\, v_{\text{st}}\, q^5} \left[q_x^2 q_y^2 + q_y^2 q_z^2 + q_z^2 q_x^2 - \frac{1}{q^2}\,(3\, q_x q_y q_z)^2\right]. \tag{2.14}$$

Here, e_{14} is the nonzero piezoelectric constant and v_{st} a mean transverse sound velocity [$v_{\text{st}} = (v_{t\,\text{fast}} + v_{t\,\text{slow}})/2$].

III. BALANCE EQUATIONS

The Liouville equation for the statistical density matrix ρ of the relative electron-phonon system is solved by considering initially decoupled relative electrons, which are in their respective thermalized stationary state described by the density matrix ρ_0 (Ref. 11)

$$\rho_0 = \frac{1}{Z_{\text{ph}}} e^{-H_{\text{ph}}/T}\, \frac{1}{Z_1} e^{-(H_{1e}-\mu_{1e}N_1)/T_{1e}} \times \frac{1}{Z_2} e^{-(H_{2e}-\mu_{2e}N_2)/T_{2e}} \tag{3.1}$$

and by turning on the interaction processes at a given time, whereas the interaction H_I itself is treated within perturbation theory. The stationary states of the decoupled systems are characterized by two electron temperatures T_{1e}, T_{2e} and two quasichemical potentials μ_{1e}, μ_{2e}. Strictly speaking, a chemical potential is not defined in this case, but this parametrization appears to be convenient for the numerical calculation. It is straightforward but cumbersome to derive the steady state energy-, force-, and particle-balance equations for the two types of carriers. We obtain

$$\begin{aligned}
\langle \dot{P}_{2x} \rangle &= n_2\, eE + F_2(v_2) + F_{\rm ph}^{21}(v_2, v_1) = 0, \\
\langle \dot{H}_{2e} \rangle &= -v_2\, F_2(v_2) - W_2(v_2) + W_{\rm ph}^{21}(v_2, v_1) = 0, \\
\langle \dot{P}_{1x} \rangle &= n_1\, eE + F_1(v_1) + F_{\rm ph}^{12}(v_1, v_2) = 0, \\
\langle \dot{H}_{1e} \rangle &= -v_1\, F_1(v_1) - W_1(v_1) + W_{\rm ph}^{12}(v_1, v_2) = 0, \\
\langle \dot{N} \rangle &= N(v_1, v_2) = 0,
\end{aligned} \tag{3.2}$$

where F_i denote the friction forces, W_i the energy losses, v_i the drift velocities, and n_i the particle numbers. The index $i = 1$ refers to 2D and $i = 2$ to 3D types of carriers, respectively.

Electron-electron interaction processes within each of the two subsystems give rise to dynamical screening of the electron-impurity and electron-phonon scattering, which is taken into account fully quantum mechanically via the random-phase approximation (RPA) for the density-density correlation function Π. Assuming a periodic potential and neglecting image contributions, we have for type 1 electrons

$$\hat{\Pi}^{(1)}(\mathbf{q}_\parallel, q_z, \omega) = \frac{\Pi^{(1)}(\mathbf{q}_\parallel, \omega)}{1 - V(\mathbf{q}_\parallel, q_z)\, \Pi^{(1)}(\mathbf{q}_\parallel, \omega)}\,, \tag{3.3}$$

where the matrix element $V(\mathbf{q}_\parallel, q_z)$ of the Coulomb potential has been calculated in Ref. 16. The dynamical RPA screening is also included in the density-density correlation function $\hat{\Pi}^{(2)}$ of type 2 electrons.

The frictional forces F and energy loss rates W of the two electronic subsystems are calculated from the following equations:

$$\begin{Bmatrix} F_1^{\rm op}(v_1) \\ W_1^{\rm op}(v_1) \end{Bmatrix} = \frac{2}{d} \sum_{\mathbf{q}\lambda} |\, M_1(\mathbf{q}\lambda)\,|^2 \begin{Bmatrix} q_x \\ \omega_{\mathbf{q}\lambda} \end{Bmatrix} |\, I_0(iq_z)\,|^2\, \hat{\Pi}_2^{(1)}(\mathbf{q}_\parallel, q_z, \omega_1 + \omega_{\mathbf{q}\lambda}) \left[n_B\left(\frac{\omega_{\mathbf{q}\lambda}}{T}\right) - n_B\left(\frac{\omega_{\mathbf{q}\lambda} + \omega_1}{T_{1e}}\right)\right], \tag{3.4}$$

$$\begin{Bmatrix} F_2^{\rm op}(v_2) \\ W_2^{\rm op}(v_2) \end{Bmatrix} = 2 \sum_{\mathbf{q}\lambda} |\, M_2(\mathbf{q}\lambda)\,|^2 \begin{Bmatrix} q_x \\ \omega_{\mathbf{q}\lambda} \end{Bmatrix} \hat{\Pi}_2^{(2)}(\mathbf{q}, \omega_2 + \omega_{\mathbf{q}\lambda}) \left[n_B\left(\frac{\omega_{\mathbf{q}\lambda}}{T}\right) - n_B\left(\frac{\omega_{\mathbf{q}\lambda} + \omega_2}{T_{2e}}\right)\right], \tag{3.5}$$

where $\omega_{1,2} = q_x v_{1,2}$ and n_B is the Bose distribution function. $\Pi_2^{(1,2)}$ are the imaginary parts of the 2D and 3D density-density correlation functions and I_0 denotes the form factor of the matrix element

$$I_0(iq_z) = \frac{\pi^2 \sin(y)}{y(y^2 - \pi^2)}\,,\ y = aq_z/2\,. \tag{3.6}$$

Furthermore, the force contributions and energy loss rates of the transfer processes are given by

$$\begin{Bmatrix} F_p^{12} \\ W_p^{12} \end{Bmatrix} = 4\pi\, |\, I(0)\,|^2 \sum_{\mathbf{q}\lambda} \sum_{\mathbf{k}_\parallel} |\, M_{12}(\mathbf{q}, \lambda)\,|^2 \begin{Bmatrix} k_x \\ \varepsilon_{1k_\parallel}/\hbar \end{Bmatrix} U(\mathbf{q}\lambda, \mathbf{k}_\parallel), \tag{3.7}$$

$$\begin{Bmatrix} F_p^{21} \\ W_p^{21} \end{Bmatrix} = -4\pi\, |\, I(0)\,|^2 \sum_{\mathbf{q}\lambda} \sum_{\mathbf{k}_\parallel} |\, M_{21}(\mathbf{q}, \lambda)\,|^2 \begin{Bmatrix} k_x + q_x \\ \varepsilon_{2k+q}/\hbar \end{Bmatrix} U(\mathbf{q}\lambda, \mathbf{k}_\parallel)\,, \tag{3.8}$$

where $|\, I(0)\,|^2 = 8a/(\pi^2 d)$ and

$$\begin{aligned}
U(\mathbf{q}\lambda, \mathbf{k}_\parallel) = {} & \left[n_F(\xi_{2\mathbf{k}+\mathbf{q}}/T_{2e}) - n_F(\xi_{1\mathbf{k}_\parallel}/T_{1e})\right] \left\{\left[n_B(\omega_{\mathbf{q}\lambda}/T) - n_B(\xi_{2\mathbf{k}+\mathbf{q}}/T_{2e} - \xi_{1\mathbf{k}\parallel}/T_{1e})\right]\, \delta(E_{2\mathbf{k}+\mathbf{q}} - E_{1\mathbf{k}\parallel} - \omega_{\mathbf{q}\lambda}) \right. \\
& \left. + \left[n_B(\omega_{\mathbf{q}\lambda}/T) - n_B(\xi_{1\mathbf{k}\parallel}/T_{1e} - \xi_{2\mathbf{k}+\mathbf{q}}/T_{2e})\right]\, \delta(E_{2\mathbf{k}+\mathbf{q}} - E_{1\mathbf{k}\parallel} + \omega_{\mathbf{q}\lambda})\right\} |_{k_z=0}\,.
\end{aligned} \tag{3.9}$$

The function U depends on the following energy variables:

$$\xi_{1\mathbf{k}\parallel} = \varepsilon_{1\mathbf{k}\parallel} - \mu_{1e}\,,\ \xi_{2\mathbf{k}} = \varepsilon_{2\mathbf{k}} - \mu_{2e}, \tag{3.10}$$

$$E_{1\mathbf{k}\parallel} = \varepsilon_{1\mathbf{k}\parallel} + k_x v_1 + \frac{m_1^*}{2} v_1^2, \tag{3.11}$$

and

$$E_{2\mathbf{k}} = \varepsilon_{2\mathbf{k}} + k_x v_2 + \frac{m_2^*}{2} v_2^2\,. \tag{3.12}$$

The restriction concerning the k_z dependence of the 3D subensemble in (3.9) is a direct consequence of our model

assumptions for the electrons in the superlattice potential. This dependence is in accordance with a qualitative discussion of the main k_z transfer contribution published by Lent, Liang, and Porod.[17]

Our main theoretical result refers to the microscopic description of the particle exchange which is calculated from the following illustrative equation:

$$
\begin{aligned}
N(v_1,v_2) = -4\pi \mid I(0) \mid^2 \sum_{\mathbf{q}\lambda} \sum_{\mathbf{k}_\parallel} \mid M_{12}(\mathbf{q},\lambda) \mid^2 \\
\times \Bigg\{ \left[1+n_B\left(\frac{\Omega_{q\lambda}}{T}\right)\right] n_F\left(\frac{\xi_{1k\parallel}}{T_{1e}}\right)\left[1-n_F\left(\frac{\xi_{2k+q}}{T_{2e}}\right)\right] \delta(E_{2k+q}-E_{1k\parallel}+\Omega_{q\lambda}) \quad \text{emission}(1\to 2) \\
+n_B\left(\frac{\Omega_{q\lambda}}{T}\right) n_F\left(\frac{\xi_{1k\parallel}}{T_{1e}}\right)\left[1-n_F\left(\frac{\xi_{2k+q}}{T_{2e}}\right)\right] \delta(E_{2k+q}-E_{1k\parallel}-\Omega_{q\lambda}) \quad \text{absorption}(1\to 2) \\
+\left[1+n_B\left(\frac{\Omega_{q\lambda}}{T}\right)\right] n_F\left(\frac{\xi_{2k+q}}{T_{2e}}\right)\left[1-n_F\left(\frac{\xi_{1k\parallel}}{T_{1e}}\right)\right] \delta(E_{1k\parallel}-E_{2k+q}+\Omega_{q\lambda}) \quad \text{emission}(2\to 1) \\
+n_B\left(\frac{\Omega_{q\lambda}}{T}\right) n_F\left(\frac{\xi_{2k+q}}{T_{2e}}\right)\left[1-n_F\left(\frac{\xi_{1k\parallel}}{T_{1e}}\right)\right] \delta(E_{1k\parallel}-E_{2k+q}-\Omega_{q\lambda}) \Bigg\} \quad \text{absorption}(2\to 1).
\end{aligned}
\tag{3.13}
$$

In our approach the complex nonlinearity of the hot-electron transport in the two-carrier system is parametrized by characteristic electron temperatures, drift velocities, and chemical potentials. According to this approximation, the electrons and phonons are still distributed via Fermi and Bose functions, respectively. Therefore, the particle number of each subsystem is obtained from

$$
n_2 = 2\sum_{\mathbf{k}} \frac{1}{\exp[(\varepsilon_{2\mathbf{k}}-\mu_{2e})/T_{2e}]+1}, \tag{3.14}
$$

$$
n_1 = 2\sum_{\mathbf{k}_\parallel} \frac{1}{\exp\left[(\varepsilon_{1\mathbf{k}_\parallel}-\mu_{1e})/T_{1e}\right]+1}. \tag{3.15}
$$

With (3.2) and (3.14), (3.15) we have a complete set of seven equations to determine the steady state values of T_{1e}, T_{2e}, v_1, v_2, μ_{1e}, μ_{2e}, and n_1 (n_2 is given by the total carrier number then).

IV. NUMERICAL RESULTS AND DISCUSSION

In order to elucidate the various influences of microscopic scattering mechanisms on the behavior of such a coupled two carrier system numerical calculations are performed for a rigid periodic square well potential. A barrier width of 100 nm and a well width of 10 nm are assumed. A donor concentration of $5\times10^{11}\,\mathrm{cm}^{-2}$ per well and $10^{15}\,\mathrm{cm}^{-3}$ in the barrier space are chosen. Such a structure is similar to a MQW system created by doping layers in GaAs, while the interlayer space is not intentionally doped.[9] Only one quantized level is assumed in the wells at a depth of 18 meV (cf. Fig. 1) and consequently a very small energy difference between the Fermi level in thermal equilibrium and the top of the barriers is obtained. Furthermore, no backcoupling of the charge transfer from the wells to the extended states is regarded with respect to the shape of the MQW potential. Despite these simplifying assumptions we believe that the essential features of the coupled system of electron gases in confined and extended states are represented. The parameters for n-type GaAs incorporated in the calculations are summarized in Table I.[18]

Due to the small energy difference between the equilibrium Fermi level and the top of the barriers, a carrier exchange between the two electronic subsystems is observed already at weak fields. Figure 2 shows the field dependence of the relative electron densities for the two-carrier systems (the inset displays the dependence at low electric fields). At $E = 0$ all electrons are confined within the wells, of course. With increasing electric fields the

TABLE I. Parameters for n-type GaAs.

Effective mass m^*/m_0	0.067
Density ρ ($g\ \mathrm{cm}^{-3}$)	5.36
Sound velocity v_s (10^5 cm/s)	5.29
Optical dielectric constant κ_∞	10.8
LO phonon energy $\hbar\omega_0$ (meV)	35.4
Static dielectric constant κ	12.9
Acoustic deformation potential E_1 (eV)	7.0 [a]
Piezoelectric constant e_{14} (10^7 V/cm)	1.41
Transverse sound velocity v_{st} (10^5 cm/s)	2.91

[a]With respect to the deformation potential constant, we use the value for bulk GaAs as in Ref. 21, too, in contrast to the enhanced values obtained in Refs. 20 and 22.

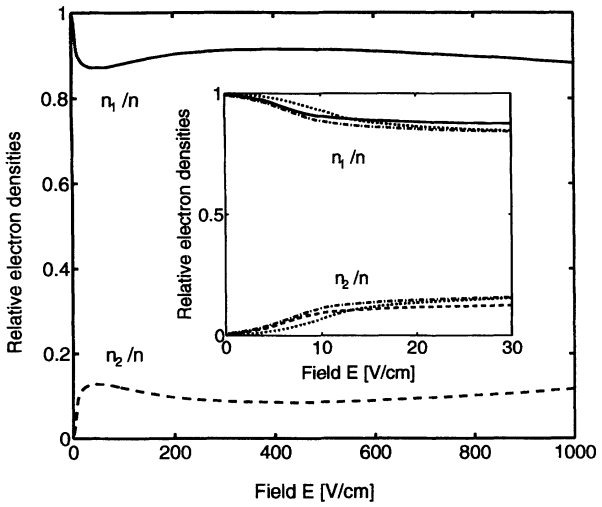

FIG. 2. Density of confined (2D, solid lines) and extended (3D, dashed lines) electrons normalized to the total electron density n as a function of the electric field. The inset shows the dependence at low electric fields. For comparison we show the result of our former approach (dotted line). The dash-dotted lines are obtained if we add all 2D electrons above E_c to the 3D carrier reservoir.

initial moderate rise of n_2 is replaced by a rapid increase of the density of electrons in the extended states. This real-space transfer of carriers tends to saturate at about 10 V/cm. Such a saturation of n_2 had also been obtained in our former approximate treatment of the carrier transfer. Evidently, this dependence seems to be general and not connected with special approximations used for the particle balance. In order to elucidate this problem we summarize the items: We had supposed that the previous approach,[9] which demanded only a constant total particle number using a single Fermi level for both subsystems, might be valid for small particle redistribution only. Therefore, we now extended the system of equations describing the transport properties for two separate entities of carriers by including the particle transfer balance explicitly and introducing separate quasi-Fermi levels in order to obtain information on a larger electric-field scale. While in detail the results of both procedures differ and this is true with respect to all calculated functions further on as they all are connected one with another, the general features are similar, for instance, the resulting tendency toward saturation of the repopulation between the subsystems already at comparatively weak electric fields. In Fig. 2, results are also shown that were obtained previously[9] (dotted line). As no microscopic transfer balance had been included in that approach we proposed that all electrons with energies above the top of the barrier be denoted as 3D carriers, whereas now they remain 2D carriers unless they are scattered into the extended states. Therefore, the number of electrons in the 3D ensemble is smaller now. To illustrate the influence of this circumstance an additional result is presented (dash-dotted line) which is obtained including the detailed particle balance as applied in the present approach but artificially denoting all carriers with energies above the top of the barrier as three-dimensional ones, delivering a similar amount as earlier (cf. dotted line). The physical background of the saturation effect appears to be determined by a sufficiently strong carrier heating in both subsystems, allowing appreciable intersubband transfer in both directions. This resembles the repopulation in the case of transfer between nonequivalent valleys,[19] which increases with enhanced energy gain from the field up to a certain amount, for which the cooler subsystem becomes sufficiently heated by phonon emission, too, leading to a decrease of the repopulation. The situation differs in the presently considered case, because the 2D electrons are transferred to extended states with a higher mobility yielding a stronger energy gain from the field. As a consequence, these carriers have a high probability of phonon assisted backscattering. Consequently, one can imagine an only weakly pronounced dependence on the applied field for the region of high carrier heating in contrast to an expected further increase. Of course, the details depend on the energetic distribution of the carriers in each subensemble and the transfer processes considered. First, a Fermi-type distribution overestimates the emission of optical phonons in the case for which electron-electron interaction no longer dominates the scattering on high-energy phonons, as probably realized for the comparatively low carrier density in the extended states. Furthermore, one should remember that only transfers assisted by acoustical phonons on account of deformation potential and by optical phonons for polar interaction are included. Scattering on ionized impurities strongly deflects the carriers from the planes of the wells into the interlayer space and, consequently, should play a remarkable role, however, with a probability that becomes less effective with increasing field strength. Concerning electron-electron collisions between the two-carrier subsystems, their impact on the particle balance cannot uniquely be predicted (see the discussion in Ref. 15).

It is interesting to compare these results for the particle numbers with the quasi-Fermi energies as functions of the field strength shown in Fig. 3 and with the field dependence of the electron temperatures depicted in Figs. 4(a) and 4(b). The circumstance that the densities of electrons in the subbands remain almost constant over a wide range of the electric field, for which the emission of optical phonons by the 3D as well as the 2D carriers is the dominating interaction mechanism, is mirrored in the quasichemical potential. Consequently, for the 2D carriers, in accordance with the estimate $n_1 \approx T_{1e} \log[\exp(\mu_{1e}/T_{1e}) + 1]$, a field independent μ_{1e} is predicted if the density n_1 is constant (and $\mu_{1e} > T_{1e}$), and vice versa. This is a peculiarity of the two-dimensional electron system that the quasichemical potential μ_{1e} is proportional to the electron density n_1 and independent of the electron temperature, as long as $\mu_{1e} > T_{1e}$ holds. Therefore, the field dependence of the electron density determines directly the quasichemical potential.

The field dependence of μ_{2e} is more complicated. From the approximation $n_2 \approx T_{2e}^{3/2} \exp(-\mid \mu_{2e} - E_c \mid /T_{2e})$ it can be estimated that for an initial moderate rise of n_2

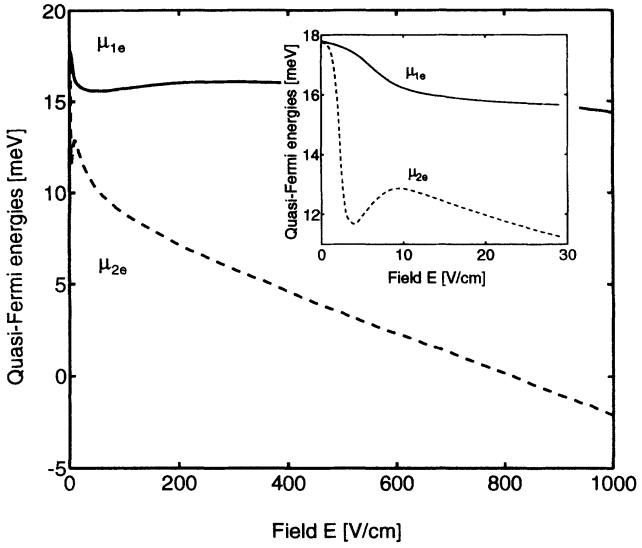

FIG. 3. Quasi-Fermi energies of confined (μ_{1e}, solid lines) and extended (μ_{2e}, dashed lines) electronic states as a function of the electric field. The inset shows the dependence at low electric fields.

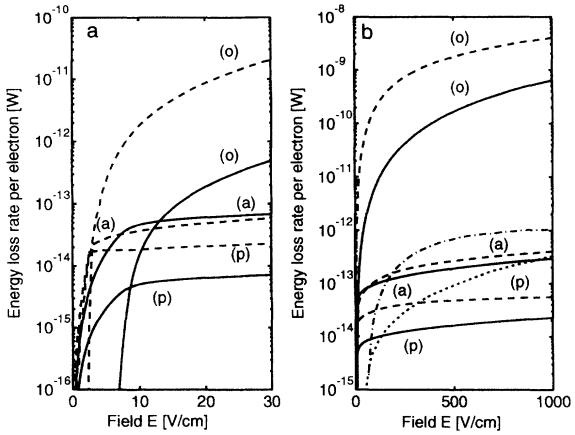

FIG. 5. Energy loss rates of confined (solid lines) and extended (dashed lines) electronic states due to scattering on polar optical (o), deformation potential (a), and piezoelectric (p) phonons. (a) shows the dependence at low electric fields. The dotted and dash-dotted lines are the contributions $-W_{\rm ph}^{12}$ and $W_{\rm ph}^{21}$, respectively.

and a rapid increase of T_{2e} (cf. Fig. 4) the quasichemical potential μ_{2e} strongly decreases. When in the adjacent field region a more pronounced carrier transfer dominates over the change of T_{2e}, one observes an increase of μ_{2e}. Above 10 V/cm, n_2 saturates and consequently μ_{2e} decreases again, however, not so rapidly because now T_{2e} increases more slowly.

In order to analyze the electron temperatures as a function of the electric-field strength, the results depicted in Fig. 4 should be compared with the energy loss rates per carrier as shown in Fig. 5 for the various electron-phonon scattering processes considered, as well as with the energy gain by the field, which is determined by the drift velocities. (In contrast to Ref. 9, the data are presented as energy loss rates per carrier in order to facilitate comparison with other publications.[20]) Up to 5 V/cm both carrier types become rapidly hot because there are only ineffective energy loss processes via acoustical phonons. The initial increase of T_{2e} is much more pronounced because the low impurity concentration between the layers allows a much higher energy gain from the electric field. At about 5 V/cm the energy relaxation of the 3D electrons by optical phonon emission sets in, which results in a slower increase of T_{2e}. Correspondingly, T_{1e} increases more slowly above about 10 V/cm due to the onset of 2D energy loss processes via optical phonons. The 3D type carriers lose much more energy than the 2D ones, which is in accordance with the much higher energy gain of the 3D electrons. From Fig. 6 it is seen that the energy

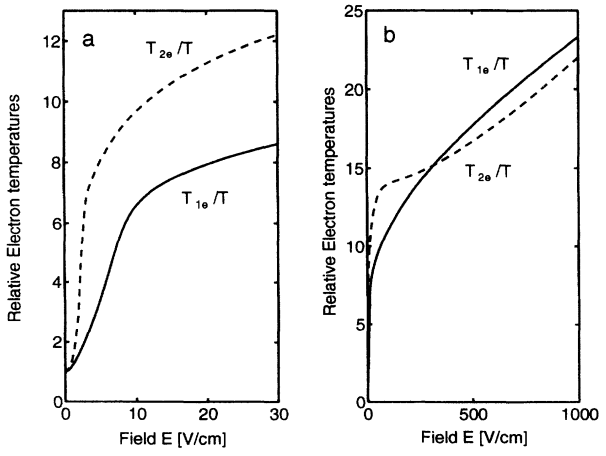

FIG. 4. Electron temperatures of confined (solid lines) and extended (dashed lines) electrons as a function of the electric field. (a) shows the dependence at low electric fields.

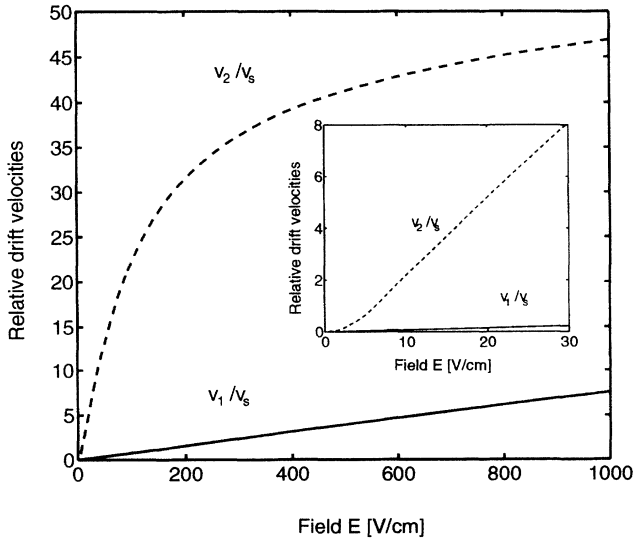

FIG. 6. Drift velocities of confined (solid lines) and extended (dashed lines) electrons normalized to the sound velocity v_s as a function of the electric field. The inset shows the dependence at low electric fields.

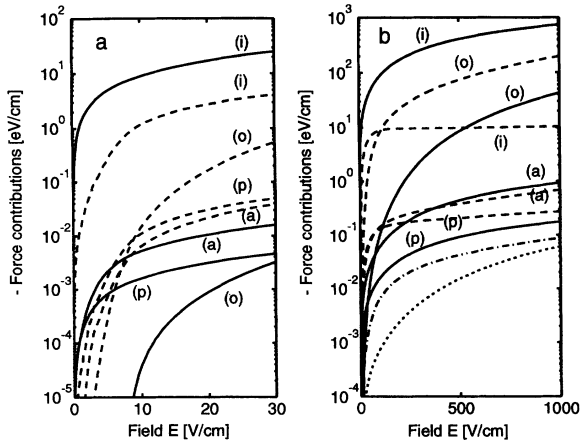

FIG. 7. Negative frictional forces of confined (solid lines) and extended (dashed lines) electronic states due to scattering on impurities (i), polar optical (o), deformation potential (a), and piezoelectric (p) phonons. (a) shows the dependence at low electric fields. The dotted and dash-dotted lines are the contributions $-F_{\rm ph}^{12}$ and $-F_{\rm ph}^{21}$, respectively.

gain of the 3D carriers tends to become less pronounced above 200 V/cm and because of the still high energy loss rate the 3D electrons seem to become even cooler than the 2D ones. This is a rather unexpected result, which can be caused by the above mentioned overestimate of the energy loss by emission of optical phonons when using a Fermi-type distribution function even if electron-electron scattering does not remain the dominating relaxation mechanism in the case of the 3D carriers with an order of magnitude less electrons than in the 2D case. Furthermore, this result depends sensitively on the set of parameters used. It should be mentioned that the slopes of the 2D and 3D electron temperatures nearly coincide above 20 V/cm.

The transfer energy-loss rates per electron $-W_{\rm ph}^{12}$ and $W_{\rm ph}^{21}$ are shown in Fig. 5(b) by the dotted and dash-dotted lines, respectively. They are always orders of magnitudes lower than the dominating loss rates.

The 2D and 3D drift velocities and frictional forces are shown in Figs. 6 and 7, respectively. As a consequence of the higher doping concentration, the impurity mediated 2D force contribution dominates over the entire electric-field region. Therefore, the corresponding drift velocity is much lower. Above 100 V/cm, the frictional force due to the scattering of 3D electrons on polar optical phonons dominates the 3D force contributions. This gives rise to a slower increase of v_2. A comparison of the v_2 data with the values obtained in Ref. 9 (which are about two times higher) shows that even the drift velocity of the 3D electrons depends sensitively on the details of the electron transfer.

The frictional forces connected with transfer processes shown in Fig. 7(b) by the dotted and dash-dotted lines are very small and can therefore be neglected in the balance equations. The differential conductivity exhibits a maximum at field strengths where the optical phonon scattering becomes dominant. This dependence was investigated both experimentally and theoretically on the basis of our former approach in Refs. 9 and 10. Because of this comprehensive discussion and the fact that all these results are qualitatively reproduced by our present approach, we skip the presentation of the corresponding data here.

V. SUMMARY

We have applied the balance-equation approach based on the separation of the center of mass from the relative motion of electrons to the electric-field driven real-space transfer of two groups of electrons in a MQW that exhibits two- and three-dimensional features, respectively. The balance equations for the energy, momentum, and particle exchange include microscopic transfer processes due to electron-phonon interaction and a full account of dynamical screening effects. Explicit analytical expressions for the particle exchange rates are given. This theory gives the microscopic foundation of our former more phenomenological approach[9,10] and allows us to consider the real-space transfer in a much larger electric-field region. We carried out numerical computations for multiple quantum wells in GaAs with a lower impurity concentration between the wells than within them and compare the results with experiments on multiple δ layers in GaAs. We assume that despite our restrictive model assumptions concerning the true MQW potential, the main physics is included in the theory presented here. The field dependence of the particle numbers, the electron temperatures, and the drift velocities are thoroughly discussed, comparing it with the behavior of the quasi-Fermi levels, the energy loss rates per electron, and the frictional forces of all considered scattering processes. This gives a detailed microscopic picture of how the numerous scattering events influence the real-space transfer of different groups of electrons. With regard to the electron repopulation between the confined and extended states, only transfer processes via electron-phonon scattering processes are taken into account; the quantitative outcome of this restriction should be further investigated by treating transfer scattering due to electron-impurity and electron-electron scattering.

We believe that the present analytical Green's function approach can be regarded as an effective tool for studying hot-electron phenomena as observed in the real-space transfer of semiconductor microstructures, too.

ACKNOWLEDGMENTS

Discussions with Professor R. Zimmermann are gratefully acknowledged.

[1] Z. S. Gribnikov, Fiz. Tekh. Poluprov. **6**, 1380 (1972) [Sov. Phys. Semicond. **6**, 1204 (1972)].
[2] K. Hess, H. Markoc, H. Shichijo, and B. G. Streetman, Appl. Phys. Lett. **35**, 469 (1979).
[3] K. Yokoyama and K. Hess, Phys. Rev. B **33**, 5595 (1986).
[4] M. Movŝko and I. Novák, J. Appl. Phys. **67**, 890 (1990).
[5] E. Schöll and K. Aoki, Appl. Phys. Lett. **58**, 1277 (1991).
[6] X. L. Lei and C. S. Ting, Phys. Rev. B **32**, 1112 (1985).
[7] H. L. Cui, X. L. Lei, and N. J. Horing, Phys. Rev. B **37**, 8223 (1988).
[8] X. L. Lei, Phys. Status Solidi B **170**, 519 (1992).
[9] H. Kostial, T. Ihn, P. Kleinert, R. Hey, M. Asche, and F. Koch, Phys. Rev. B **47**, 4485 (1993).
[10] M. Asche, R. Hey, M. Höricke, T. Ihn, P. Kleinert, H. Kostial, B. Danilchenko, A. Klimashov, and S. Roshko, Semicond. Sci. Technol. **9**, 835 (1994).
[11] X. L. Lei, D. Y. Xing, M. Liu, C. S. Ting, and J. L. Birman, Phys. Rev. B **36**, 9134 (1987).
[12] D. Y. Xing, M. Liu, P. Hu, and C. S. Ting, J. Phys. C **21**, 2881 (1988).
[13] M. Babiker, Semicond. Sci. Technol. **7**, B52 (1992).
[14] S. D. Sarma, V. B. Campos, M. A. Stroscio, and K. W. Kim, Semicond. Sci. Technol. **7B**, 49 (1992).
[15] M. J. Martisov and A. J. Shik, Fiz. Tekh. Poluprov. **21**, 1474 (1987) [Sov. Phys. Semicond. **21**, 896 (1987)].
[16] X. L. Lei, N. J. M. Horing, and J. Q. Zhang, Phys. Rev. B **34**, 1139 (1986).
[17] C. S. Lent, L. Liang, and W. Porod, Appl. Phys. Lett. **54**, 2315 (1989).
[18] X. L. Lei, J. L. Birman, and C. S. Ting, J. Appl. Phys. **58**, 2270 (1985).
[19] M. Asche, B. I. Boichenko, V. M. Bondar, and O. G. Sarbey, Phys. Stat. Solidi B **44**, 173 (1971).
[20] K. Hirakawa and H. Sakaki, Appl. Phys. Lett. **49**, 889 (1986).
[21] A. J. Vickers, Phys. Rev. B **46**, 13 313 (1992).
[22] S. Manion, M. Artaki, M. A. Emanuel, J. J. Coleman, and K. Hess, Phys. Rev. B **35**, 9203 (1987).